



1 Meteorological formation mechanism of regional transport in winter 2 heavy air pollution events in the middle Yangtze River area, China

3
 4 Yongqing Bai¹ Tianliang Zhao^{2*} Yue Zhou^{1*} Jie Xiong¹ Weiyang Hu² Yao Gu² Lin Liu¹
 5 Shaofei Kong³ Huang Zheng³

6
 7 1. Hubei Key Laboratory for Heavy Rain Monitoring and Warning Research, Institute of Heavy Rain, China
 8 Meteorological Administration, Wuhan 430205, China
 9 2. Key Laboratory for Aerosol-Cloud-Precipitation of China Meteorological Administration, Nanjing University of
 10 Information Science and Technology, Nanjing 210044, China
 11 3. Department of Atmospheric Science, School of Environmental Studies, China University of Geosciences
 12 (Wuhan), 430074

13
 14 Correspondence: Tianliang Zhao (josef_zhao@126.com) and Zhou Yue
 15 (zhouyue8510@163.com)

16
 17 **Abstract:** Anthropogenic emission, meteorological conditions, and regional transport
 18 are the three major factors influencing heavy air pollution in China. The Hunan and
 19 Hubei provinces in the middle Yangtze River region border China's main air pollution
 20 areas, serving as the hub of regional transport of air pollutants. The meteorological
 21 formation mechanism of regional transport of air pollutants on heavy air pollution in
 22 the Hunan and Hubei provinces still remain urgent to be addressed in depth. In this
 23 study, multivariate empirical orthogonal function (MV-EOF) analysis was performed
 24 to objectively select eight typical heavy pollution events in the two provinces that
 25 occurred in January 2015–2019. Based on the regional surface environment,
 26 meteorological network data, atmospheric sounding data, ERA-interim reanalysis data,
 27 and a numerical simulation experiment, this study investigated the pattern of regional
 28 transport of air pollutants in the two provinces and its mechanism of regional
 29 meteorological conditions. The results showed that transporting air pollutants mainly
 30 passed through two transport pathways, namely the Nanxiang Basin-Yunmeng Plain
 31 pathway and the Dabie Mountain's Hilly Area-Yunmeng Plain pathway, existing
 32 anomalous near-surface northerly winds in the two provinces and their upstream area
 33 accompanied by southward penetration of a shallow cold layer, all of which jointly
 34 provide a dynamic condition for regional air pollutant transport. The weak cold-air
 35 mass degenerated as it passed through the Hunan–Hubei Plain, causing warm air to



36 accumulate in the near-surface layer of the downstream area, where winds slowed
37 down and converged, buffering the air pollutant transport and resulting in pollutants
38 accumulation; the near-surface atmosphere of the Hunan and Hubei provinces was a
39 non-stagnant condition (dry intrusion of cold air, anomalous northerly winds, and
40 positive anomalies of boundary-layer height), which is conducive to the horizontal
41 transport of air pollutants. However, the mid-high layers, characterized by
42 temperature inversion and the presence of a "warm lid", had a stable stratification,
43 inhibiting the diffusion of air pollutants to the upper layers; there is an obvious
44 longitudinal vertical circulation above the Hunan–Hubei Plain, which results in the
45 sinking and accumulation of air pollutants, thereby promoting rapid accumulation of
46 air pollutants in the Hunan and Hubei provinces. In addition, extended empirical
47 orthogonal function (EEOF) analysis was performed, revealing a quasi-4-d periodic
48 oscillation pattern of air pollutants transport in the Hunan and Hubei provinces, which
49 provides a reference for early prediction of its regional transport. The findings are of
50 practical value in broadening the scientific understanding of the differences in the
51 formation mechanism of heavy atmospheric pollution between the various regions of
52 China and promoting environmental and ecological protection of the middle Yangtze
53 Basin.

54

55 **1 Introduction**

56 At present, China is facing a severe air pollution situation, and in particular,
57 regional atmospheric environmental problems characterized by the pollution of
58 inhalable particulate matter (PM₁₀) and fine particulate matter (PM_{2.5}) are increasingly
59 prominent, which is the main challenge in China's atmospheric environmental
60 management (Kan et al., 2012; Zhao et al., 2013; Zhang et al., 2015). Under certain
61 geographical and meteorological conditions, atmospheric pollutants diffuse and
62 accumulate on a certain spatial scale. Air pollutants flow freely between cities and
63 urban agglomerations and undergo trans-boundary transport, characterized by a
64 combination of regional pollution and compound pollution, with regional joint
65 prevention and control of pollutant transport becoming the focus of atmospheric
66 environmental issues in China (Wu et al., 2013b; Miao et al., 2017; Lu et al., 2019a).
67 Exploring meteorological mechanism of regional air pollutant transport, scientifically
68 assessing the atmospheric environmental changes, and effectively regulating pollutant
69 emissions constitute an important topic of atmospheric environmental research



70 (Cheng et al., 2019; Zhang et al., 2019; Huang et al., 2020).

71 China's heavy atmospheric pollution often occurs in winter, and the
72 pollution-promoting meteorological conditions in winter are usually about 40-100%
73 worse than those in other seasons (Zhang et al., 2018). The effects of
74 meteorological conditions on the formation, distribution, maintenance, and change of
75 aerosol pollution are significant (Tai et al., 2012; Ding et al., 2016; Guo et al., 2019).
76 Excessive anthropogenic emission, stable meteorological conditions, and regional
77 transport of air pollutants are important factors in the formation of heavy air pollution
78 (Zhang et al., 2012a; Guo et al., 2016a; Ning et al., 2018). Under stagnant
79 meteorological conditions, weak winds, strong and thick temperature inversion layers,
80 sinking motion and low mixing layer heights are extremely unfavourable for the
81 diffusion of air pollutants, with these local meteorological conditions acting as an
82 external driver for the formation of heavy air pollution (Wang et al., 2013a; Xu et al.,
83 2016; Guo et al., 2016b; Ding et al., 2017).

84 Regional transport of air pollutants involves complex atmospheric physical and
85 chemical processes and is influenced by many factors such as meteorological
86 background field, topography, distribution of emission sources, and atmospheric
87 chemical transformation (Wang et al., 2013b). The transport and accumulation of air
88 pollutants result from the interaction between topographic conditions and
89 meteorological conditions (Zhang et al., 2012b). Air pollutant transport under the
90 control of the cold front system has a significant impact on the atmospheric level of
91 PM_{2.5} in Shanghai in winter (Xu et al., 2016). The weather processes leading to heavy
92 pollution in Hong Kong mainly involve the transport of high-concentration aerosols
93 carried by cold air (Yang et al., 2019). In the Pearl River Delta, 50-70% of PM_{2.5}
94 originates from long-distance transport, resulting in more severe pollution in the
95 suburbs than in the nearby urban areas (Wu et al., 2013a). During the aerosol
96 accumulation stage, PM_{2.5} concentration in the Beijing-Tianjin-Hebei region increased
97 from 24.2 to 289.8 $\mu\text{g m}^{-3}$, with the contributions of regional transport increasing
98 from 12 % to 40 %, while the contribution of local emissions decreased from 59 % to
99 38 % (Chen et al., 2019). The rapid changes in the formation and dissipation process
100 of heavy pollution in Beijing are mainly caused by the regional transport and the
101 alternation between northerly and southerly air masses (Gao et al., 2016), and the
102 regional transport is estimated to contribute to as much as 53%-70% in the explosive
103 growth period of PM_{2.5} (Li et al., 2017a). Fine particulates can be transported across a



104 wide range and over a long distance with obvious trans-boundary transport
105 characteristics, which has an important effect on the dynamics of atmospheric
106 pollution (Kim et al., 2012; Khuzestani et al., 2017; Li et al., 2019; Yuan et al., 2019).

107 Hunan and Hubei provinces in the middle Yangtze River area have a special
108 geographic location, forming the border of China's most concentrated areas of
109 atmospheric pollution—the Central Plains, Fenwei Plain, North China Plain, and
110 Yangtze River Delta region. Hunan and Hubei provinces are located in the downwind
111 direction of the areas of heavy air pollution sources under the influence of winter
112 monsoon, serving as a hub for the regional transport of air pollutants (Figure 1). The
113 mechanism of regional air pollutant transport on the air pollution in the Hunan–Hubei
114 Plain is a pressing issue of atmospheric environmental science calling for in-depth
115 investigation. With the development of China's Yangtze River Economic Belt and
116 middle Yangtze Basin, the atmospheric environment problems in Hunan and Hubei
117 provinces have become increasingly prominent. Different from cumulative heavy
118 pollution in central and eastern China, the pollutant-transport characteristics and the
119 effect mechanism of meteorological conditions on heavy pollution processes in
120 typical regions like Hunan and Hubei provinces have not yet been systematically
121 investigated. To fill the knowledge gap, this study employed regional surface
122 environment data, meteorological network data, atmospheric sounding data, and
123 ERA-interim reanalysis data in combination with synthetic analysis, climate diagnosis,
124 and numerical simulation to comprehensively investigate the mechanism of air
125 pollutant transport on the process of heavy air pollution in winter in Hunan and Hubei
126 provinces. The findings are of practical value in broadening the scientific
127 understanding of the formation mechanism differences of heavy atmospheric
128 pollution between various regions of China and promoting environmental and
129 ecological protection of the middle Yangtze River area.

130

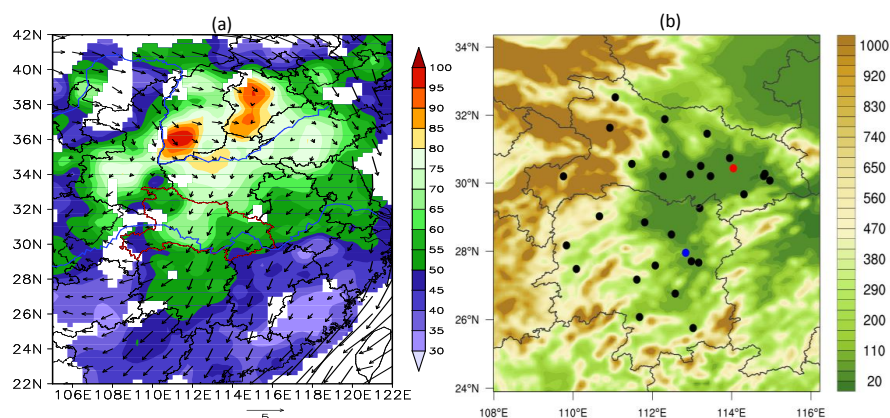


Figure 1 (a) Distribution of average PM_{2.5} concentration (colour scale, in $\mu\text{g m}^{-3}$) and average ERA-interim 10-m wind vectors (denoted by arrows, in m s^{-1}) measured at the environmental monitoring stations of central and eastern China in January 2015-2019, and (b) topographic map of the distribution of environmental monitoring stations in 31 cities of Hunan and Hubei provinces (colour scale, in m), where the red point represents the Wuhan station, and the blue point represents the Changsha station.

2 Data and methods

2.1 Data source

The daily average PM_{2.5} concentration in January 2015-2019 was obtained from China's National Ambient Air Quality Monitoring Network, which can be accessed through the data centre of the Ministry of Ecology and Environment (<http://datacenter.mee.gov.cn/>). For the same period, the hourly data of the surface meteorological elements such as sea level pressure (SLP), 2-m air temperature, and 10-m wind speed and wind direction, as well as the atmospheric sounding data of temperature and wind speed at 00 UTC each day at the Wuhan station and Changsha station, were sourced from China Meteorological Data Network (<http://data.cma.cn/>).

Moreover, the contemporary ERA-interim daily reanalysis data were obtained (<http://apps.ecmwf.int/datasets/data/>) with a resolution of $0.25^\circ \times 0.25^\circ$ consisting of the atmospheric boundary-layer height, SLP, 2-m air temperature, 10-m wind vector components u and v at 00 UTC each day, as well as the geopotential height, temperature, vertical speed, and wind vector components u and v at different vertical layers at 00 UTC each day.



2.2 Multivariate and extended empirical orthogonal function decomposition (MV-EOF, EEOF)

The multivariate empirical orthogonal function decomposition (MV-EOF) is essentially the same as extended empirical orthogonal function decomposition (EEOF). They are both based on the classical empirical orthogonal function decomposition (EOF) to extend the spatial dimension of original data matrix in a different manner, that is, MV-EOF allows extension of multiple elements, while EEOF allows extension of multiple consecutive time points.

When using MV-EOF to study the spatio-temporal variation of the transport modes of pollutants, it is necessary to consider the eigenvectors of a combined ensemble of pollutant data and wind pressure field data. By extending the spatial dimension of $PM_{2.5}$ and wind pressure fields, it is possible to derive the distribution of typical multivariate modes and their time coefficients.

The EOF decomposition can reveal the spatial distribution structure of the element field, but the revealed structure is in a time-invariant form, failing to provide a time-dependent spatial distribution structure under disturbance. Based on the significant temporal autocorrelation of element field, EEOF can extend the original data matrix into observation data corresponding to multiple consecutive time points using a certain lag time, so that the time-dependent spatial distribution characteristics and regional transport patterns of pollutants can be obtained. When using EEOF to analyse the quasi-periodic oscillation and evolution characteristics of the region transport of $PM_{2.5}$, it is necessary to first separate the specific periodic components in the element field of $PM_{2.5}$, and then, perform EEOF decomposition on the separated data. The significant periods in the time series of $PM_{2.5}$ can be extracted using a power spectrum method, and the separation of specific periodic components from the element field can be achieved via a second-order Butterworth band-pass filter.

Moreover, other statistical methods such as synthetic analysis and correlation analysis were also applied in this study. It is noteworthy that the anomalies of each element used in the synthesis of a typical example were calculated using the average meteorological values in January 2015–2019.

3 Selection of regional air pollutant transport events

There are three main causes of heavy air pollution, namely anthropogenic



emissions far exceeding the environmental carrying capacity, unfavourable meteorological conditions, and regional transport of air pollutants. The local meteorological conditions leading to heavy cumulative pollution mainly include (1) poor air mobility and calm surface winds or small surface winds (wind speed less than 2 m s^{-1}), which are extremely unfavourable for the horizontal diffusion of pollutants; (2) stable atmospheric conditions, near-surface temperature inversion, and significant decrease of boundary-layer height, which are unfavourable for the vertical distribution of air pollutants. In contrast to the above conditions are the meteorological conditions leading to regional transport of heavy air pollution, which mainly include obviously enhanced surface winds and favourable horizontal diffusion conditions; under these transport-facilitating conditions, the pollutant concentration rises, which is mainly attributed to pollutant transport from the upstream areas, that is, the regional transport promotes a rapid local accumulation of pollutants.

The atmospheric circulation during the East Asian winter monsoon drives the regional transport of air pollutants in central and eastern China and facilitates the accumulation of air pollutants in the middle reaches of the Yangtze River (Yu et al., 2020). The $\text{PM}_{2.5}$ concentration in Wuhan usually rises rapidly under the influence of strong northerly winds (Lu et al., 2017, 2019b). The regional transport of air pollutants in the middle Yangtze River region is dominated by near-surface northerly airflow, which is air pollutant transport from northern China (Yue et al., 2016; Li et al., 2019; Xiao et al., 2020). As shown above, the transported air pollutants in Hunan and Hubei provinces is characterized by high regional concentration of $\text{PM}_{2.5}$, north–south pressure gradient, and anomalous northerly winds. Therefore, MV-EOF was adopted in this study to extract the common eigenvectors and time coefficients of four variables—daily average $\text{PM}_{2.5}$ concentration, 10-m wind vector components U and V, and SLP (00 UTC each day) in January 2015–2019 at 31 urban environmental monitoring stations of Hunan and Hubei provinces.

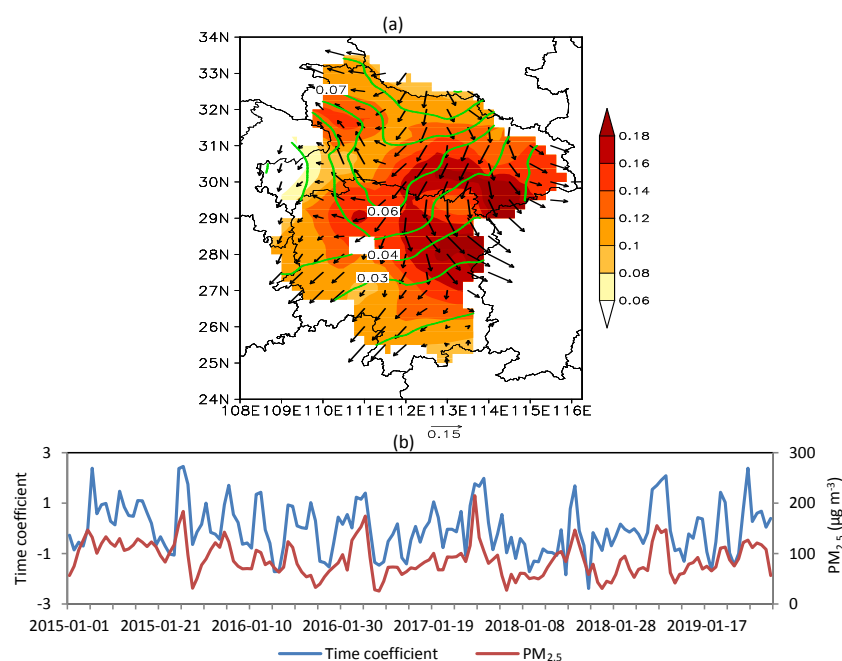
Figure 2 presents the spatial distribution and time coefficients of the MV-EOF mode featured by high $\text{PM}_{2.5}$ concentration, south–north pressure gradient, and anomalous northerly winds for the regional pollutant transport in Hunan and Hubei provinces. In particular, the Wuhan-centred urban agglomeration and Changsha–Zhuzhou–Xiangtan urban agglomeration had the most obvious spatial characteristics. This mode accounted for 12% of the total variance, and its time coefficient accounted for 48.4% of the total variance of the time series of daily averaged $\text{PM}_{2.5}$ in the two



provinces, indicating that regional transport was almost the most dominant factor determining the changes in pollutant concentrations in the Hunan and Hubei provinces. After normalization of the time coefficient, eight typical regional transport events with maximum standard deviation of time coefficient were selected to explore the meteorological conditions leading to regional transport of heavy pollution in the Hunan and Hubei provinces (Table 1).

230

231



232

Figure 2 Spatial distribution of the MV-EOF mode (a) of $PM_{2.5}$ denoted by the colour scale, of wind vector with components U and V represented by arrows, and of SLP displayed by green contour lines (all the elements are dimensionless), and (b) its time coefficient and the time series of regional mean $PM_{2.5}$ concentration (in $\mu g m^{-3}$).

237

Table 1 Eight typical regional pollutant-transport events in the Hunan and Hubei provinces

239

No.	typical regional transport events (standard deviation of time coefficient)	regional mean $PM_{2.5}$ concentration (anomalies) ($\mu g m^{-3}$)	regional mean wind speed (anomalies) ($m s^{-1}$)	start and end of regional transport
1	Jan. 6, 2015 (2.38)	135 (45)	2.9 (2.1)	Jan. 4-7, 2015
2	Jan. 25, 2015 (2.37)	161 (71)	1.6 (0.7)	Jan. 23-27, 2015



3	Jan. 26, 2015 (2.46)	185 (95)	0.9 (0.1)	Jan. 24-27, 2015
4	Jan. 5, 2016 (1.71)	123 (33)	2.4 (1.6)	Jan. 3-6, 2016
5	Jan. 30, 2017 (1.98)	104 (14)	2.5 (1.7)	Jan. 28-31, 2017
6	Jan. 7, 2019 (1.91)	143 (53)	1.5 (0.7)	Jan. 4-9, 2019
7	Jan. 8, 2019 (2.09)	146 (56)	1.2 (0.4)	Jan. 5-9, 2019
8	Jan. 26, 2019 (2.38)	125 (34)	1.7 (0.9)	Jan. 24-27, 2019

4 Air pollutant transport characteristics in Hunan and Hubei provinces and mechanism of meteorological conditions on the heavy air pollution process

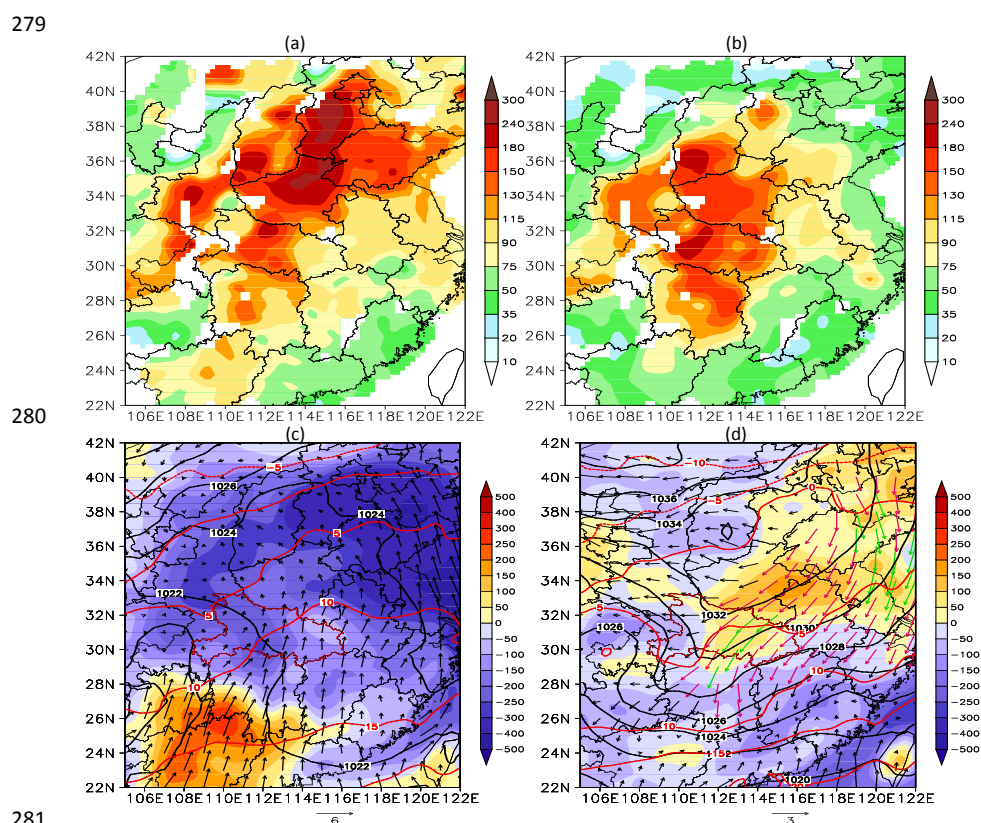
4.1 Air pollutant transport and the predictive regional characteristics

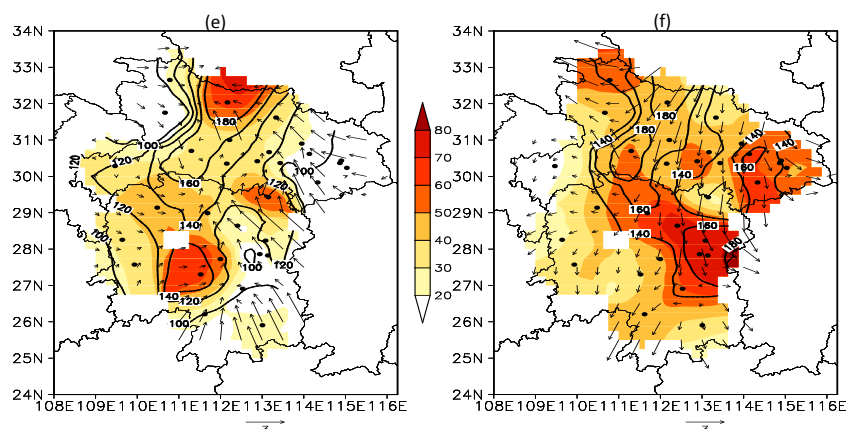
Figure 3 presents the spatial distribution of regional $PM_{2.5}$ concentration, anomaly, and surface synoptic situations obtained from eight typical pollutant-transport events on the onset day (0d) and two days earlier (-2d), respectively. As shown in the figure, the region at -2d was under the influence of a uniform pressure field and low air pressure, and a large range of stagnant weather patterns appeared in northern and central China, including an obvious characteristic of small southerly winds and calm winds, an obvious decrease in the atmospheric boundary-layer height, and a weak diffusion of pollutants in the horizontal and vertical directions, all jointly resulting in local cumulative heavy pollution. In particular, the air pollutant concentration was the highest in northern China and the Central Plains, with local $PM_{2.5}$ concentrations exceeding $250 \mu g m^{-3}$, whereas the local air pollutant accumulation in Hunan and Hubei provinces occurred at a relatively low level.

On the onset day of regional transport, atmospheric circulation underwent changes, that is, the surface south–north pressure gradient was enhanced. Affected by the lower part of the surface high-pressure system, the eastern cold air, which was dominated by north-easterly winds moved southwards, and the 2-m air temperature was reduced. The wind speeds in the two provinces and their upwind areas were increased obviously, and the atmospheric boundary layer was significantly elevated, with the Hunan–Hubei Plain located at the centre of an anomalous northerly wind belt. On the contrary, the wind speed in southern China was weakened and buffered the northerly airflow, which promoted the horizontal transport and accumulation of near-surface pollutants in the Hunan and Hubei provinces. With respect to pollution evolution over different regions, the $PM_{2.5}$ concentration in northern China and the Central Plains decreased, whereas the $PM_{2.5}$ concentration in the Hunan and Hubei provinces increased.



269 With respect to the observed anomalous wind fields and $\text{PM}_{2.5}$ concentration
 270 distribution in Hunan and Hubei provinces (Figure 3e, f), there existed anomalous
 271 southerly winds in the early stage, accompanied by local pollutant accumulation;
 272 when regional air pollutant transport occurred, the wind fields turned into anomalous
 273 northerly winds, which resulted in increased air pollutant concentration in the Hunan–
 274 Hubei Plain, especially in the Wuhan-centred urban agglomeration and the Changsha–
 275 Zhuzhou–Xiangtan urban agglomeration where most areas experienced more than 50
 276 $\mu\text{g m}^{-3}$ of $\text{PM}_{2.5}$ concentration anomalies, indicating that regional transport of air
 277 pollutants would increase the rapid local accumulation of air pollutants in these
 278 high-density cities.





282

283 Figure 3 The spatial distribution of daily mean $\text{PM}_{2.5}$ concentration (in $\mu\text{g m}^{-3}$) in
 284 central and eastern China on the onset day (b) of eight typical pollution events and
 285 two days earlier (a); weather maps at the surface from the ERA-interim daily dataset
 286 for central and eastern China on the onset day (d) and two days earlier (c), where the
 287 colour scale indicates the anomalies (in m) of atmospheric boundary-layer height, the
 288 black contour lines represent SLP (hPa), the red contour lines represent the 2-m air
 289 temperature (in $^{\circ}\text{C}$), the arrows denote anomalous wind fields (in m s^{-1}), the red
 290 arrows represent more than 1.5 m s^{-1} of anomalies of wind speed, and the green arrow
 291 represents more than 2.5 m s^{-1} of anomalies of wind speed; spatial distribution of the
 292 daily mean $\text{PM}_{2.5}$ concentration (black contour lines, in $\mu\text{g m}^{-3}$) and anomalies (colour
 293 scale, in $\mu\text{g m}^{-3}$) as well as anomalous wind fields (arrows, in m s^{-1}) on the above
 294 onset day (f) and two days earlier (e) in the Hunan and Hubei provinces, with data
 295 from the observation stations of the two provinces.

296

297 Figure 4 shows the spatial distribution of 10-m wind speed observed at
 298 nationwide observation stations at 00UTC on the onset day of eight typical
 299 pollutant-transport events and the spatial distribution of 24-h temperature changes
 300 observed at the above stations. As shown in the diagrams, the Hunan and Hubei
 301 provinces as well as most of the eastern upstream area experienced a wind speed
 302 above 2 m s^{-1} , and the pollutants mainly passed through two transport pathways,
 303 namely the Nanxiang Basin-Yunmeng Plain pathway and the Dabie Mountain's Hilly
 304 Area-Yunmeng Plain pathway, where the local winds moved at a speed of above 3.5
 305 m s^{-1} , transporting air pollutants towards the Hunan–Hubei Plain. The dynamic
 306 conditions for regional pollutant transport were triggered by the southward movement



of weak cold air, which was similar to the process of a cold front system causing air pollutant transport from northern China to the Yangtze River Delta region (Kang et al., 2019). Under the influence of cold air, most of the northern regions experience temperatures of -5 to -2 °C within 24 h, and the 24-h temperature changes in Hunan and Hubei provinces were -3 to -2 °C. Because of the weak southward cold air, its influence exists as far as only the Hunan province. After passing through the Hunan–Hubei Plain, the cold air degenerates, and the Guangdong-Guangxi hilly regions and Zhejiang-Fujian hilly regions in the south undergo positive temperature changes of 0-2 °C, so wind speed reduces in these areas, causing air pollutants to stagnate and accumulate in the Hunan–Hubei Plain. As shown above, short-term activities of weak cold air are crucial for pollutant transport in the Hunan and Hubei provinces.

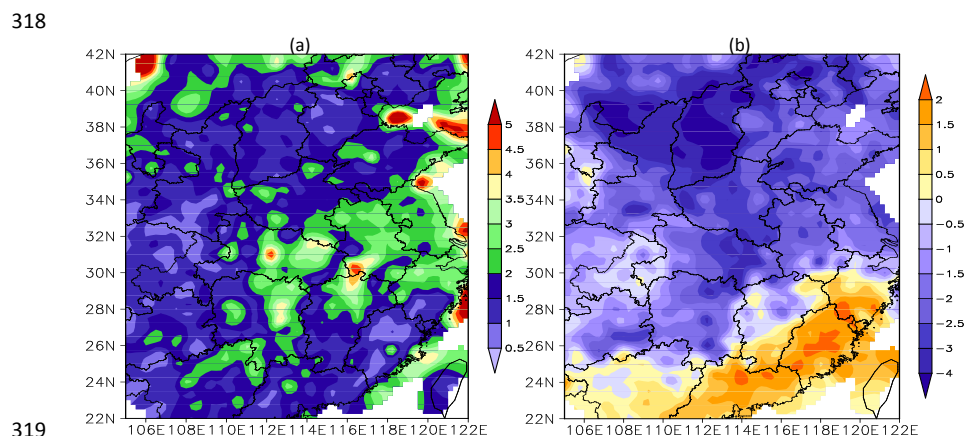


Figure 4 Spatial distribution of surface 10-m wind speeds (in m s^{-1}) during eight typical pollution events (a) and spatial distribution of 24-h temperature changes (in °C) during the above events, with the data from nationwide observation stations at 00 UTC.

4.2 Circulation characteristics affecting regional transport

Figure 5 represents the spatial distribution of the correlation coefficient between the time series (sequences in Figure 2b) of a mode of regional pollutant transport and some meteorological parameters (SLP, boundary-layer height, and 10-m wind vector with components U and V) to verify the association between regional pollutant transport and surface synoptic situation. The results indicate that consistent with the analysis results of Figure 2d, the favourable meteorological conditions for air pollutant transport in the Hunan and Hubei provinces include anomalous northerly



winds under the influence of the lower part of a surface high-pressure system and a high atmospheric boundary layer in the transport pathways of the Hunan–Hubei Plain and in its upstream area, all of which are conducive to diffusion and transport of air pollutants.

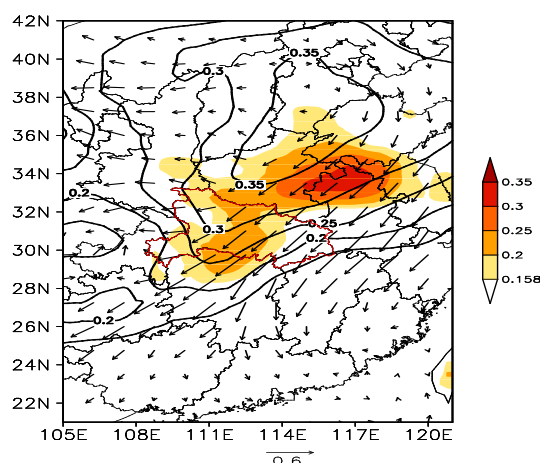


Figure 5 Spatial distributions of the correlation coefficients between the regional transport mode time coefficient and the meteorological parameters (SLP, boundary-layer height and 10-m wind vector) during the same period. The correlation coefficients of SLP denoted by black contour lines, the correlation coefficients of boundary-layer height denoted by the colour scale, and the correlation coefficients of 10-m wind vector denoted by arrows.

Figure 6 presents the surface synoptic situation and the synoptic situation at higher layers (850 hPa, 700 hPa, and 500 hPa) caused by eight typical pollutant-transport events. As shown in the figure, affected by the anomalous northerly airflow under the influence of the lower part of the surface high-pressure system in northern China, weak cold air penetrated southward to central China, driving air pollutants from the northern source areas to Hunan and Hubei provinces. The southward airflow showed a weaker convergence in southern and eastern China; moreover, warm air masses converged in the Hunan and Hubei provinces, acting as a buffer, so air pollutants were stagnated and accumulated in the Hunan–Hubei Plain, which accelerated the rapid local accumulation of pollutants. The synoptic situation at 850 hPa was similar to that of the surface, that is, the anomalous northerly winds carried the north-sourced pollutants to Hunan and Hubei provinces, and the



convergence zone with positive anomalies of temperature tended to be uplifted northward, which made the upper atmospheric layer over the Hunan and Hubei provinces tend to be in a stable condition. At the mid-high layers of 700 hPa and 500 hPa, Hunan and Hubei provinces and their upstream area were markedly characterized by the presence of a “warm lid” under the influence of positive geopotential height anomalies, which prevented pollutants from diffusing to higher atmospheric layers during the transport process; moreover, a warm high-pressure system existed in the mid-high layers. All these characteristics indicated that it was a weak cold air system with a shallow boundary layer.

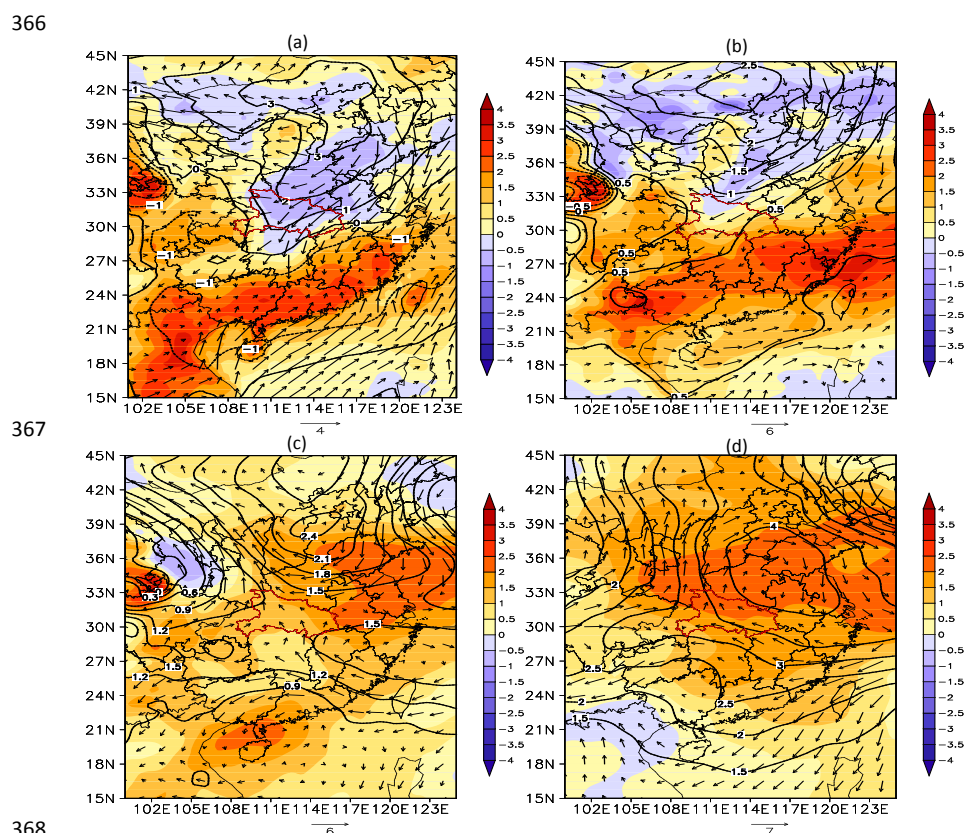


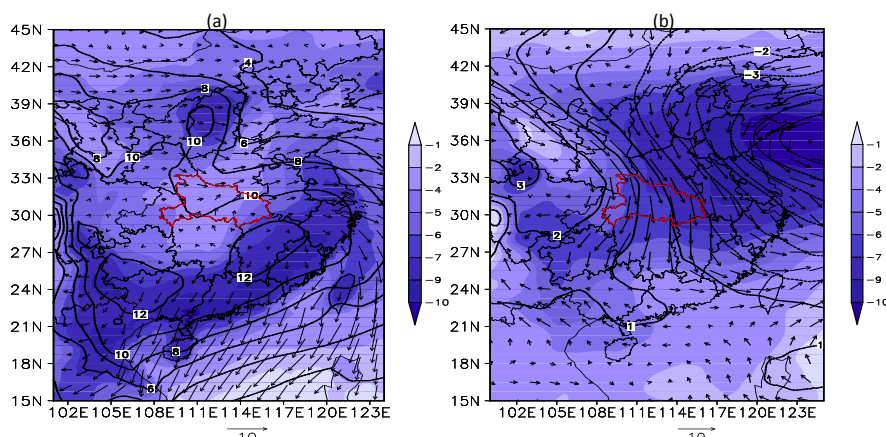
Figure 6 The surface synoptic situation (a) and the synoptic situation at higher layers of 850 hPa (b), 700 hPa (c), and 500 hPa (d) synthesised from eight typical pollutant-transport events. The black contour lines represent the anomalies of surface SLP (in hPa) and high-altitude geopotential height (in dagpm); the colour scale represents temperature anomalies (in °C); the arrows represent anomalous wind fields (in m s^{-1}) from the ERA-interim daily dataset at 00:00 UTC.



375

376 The atmospheric circulation situation on pollution-free days showed that strong
 377 cold-air advection with strong winds would have an obvious positive effect on the
 378 removal of air pollutants. To better understand the differences between the
 379 meteorological conditions for air pollutant transport into the Hunan and Hubei
 380 provinces and the meteorological conditions for air pollutant removal from the region,
 381 the synoptic situation for strong winds to remove pollution was synthesized from
 382 eight events in which air pollutants were removed by strong winds. Next, the
 383 element-wise differences of the synoptic situation between the above two types of
 384 events were calculated, as shown in Figure 7. For the surface synoptic situation, there
 385 was no significant difference in the 10-m wind vectors between the two types of
 386 events in the Hunan and Hubei provinces, but in the case of strong winds removing
 387 the pollutants, the cold high-pressure system in northern China was stronger, with
 388 strong cold airflow sweeping across the Hunan and Hubei provinces and directly
 389 affecting the coastal areas of southern and south-eastern China. The wind speeds in
 390 the coastal areas were anomalously high, where no warm air masses converged to
 391 buffer pollutant transport, so air pollutants failed to accumulate in the Hunan and
 392 Hubei provinces. Moreover, the differences in the synoptic situation at the mid-high
 393 layers indicated that when strong winds were removing the air pollutants, the
 394 northerly winds were stronger, the cold air masses were thicker, and no stationary
 395 atmospheric states could be formed in the mid-high layers above Hunan and Hubei
 396 provinces, which facilitated vertical diffusion of pollutants.

397



398

399 Figure 7 Element-wise differences in synthesized synoptic situations between eight

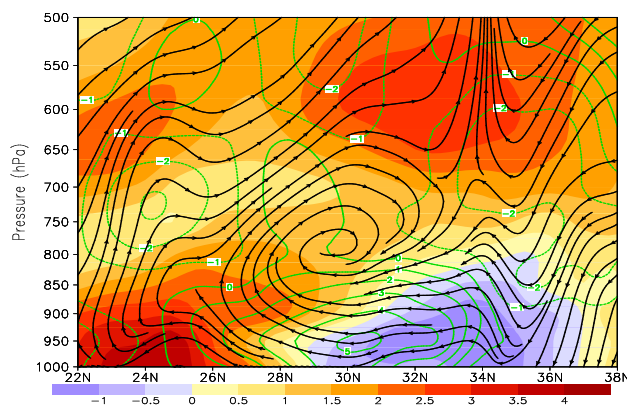


400 events of big wind-induced pollutant removal and eight events of big wind-induced
401 pollutant input at the surface (a) and the atmospheric layer of 700 hPa (b), with the
402 black contour lines representing the surface SLP differences (in hPa) and the
403 high-altitude geopotential height differences (in dagpm), the colour scale representing
404 the temperature differences (in °C), and the arrows representing the wind field
405 differences (in m s^{-1}) from the ERA-interim daily dataset at 00:00 UTC.

406

407 **4.3 Influence of atmospheric vertical structure on regional transport**

408 Figure 8 presents the longitudinal cross-sectional structure of the pollutant-transport
409 channel along the Hunan–Hubei Plain (synthesised from eight typical
410 pollutant-transport events). There was a clear longitudinal vertical circulation above
411 the plain, which spanned the latitudes of 26.5°N–32.5°N and vertically extended to
412 the layer of 650 hPa, with the central height corresponding to an air pressure of 800
413 hPa. The mid-high layers above the 800-hPa layer were dominated by weak southerly
414 airflow, whereas below the 800-hPa layer, strong northerly airflow was observed, with
415 wind speed anomalies reaching 2–5 m s^{-1} . The northerly airflow rose in the south of
416 the plain, but it underwent circulation and sank in the north of the plain. The
417 longitudinal vertical circulation structure was triggered by the southward penetration
418 of the weak cold air with a shallow boundary layer. The southward moving weak cold
419 air was wedged into the bottom of the warm air, and the warm air was uplifted, not
420 only leading to stable stratification similar to that in the frontal zone but also forming
421 a high-altitude “warm lid” above the Hunan–Hubei Plain and the upstream area,
422 which suppressed the vertical diffusion of pollutants during their transport. The cold
423 air exhibited weak activity, and wind speed anomalies turned negative in the
424 downstream area, where warm air was squeezed and underwent convergence, rising
425 and moving northward in a roundabout manner. Later, the warm air transformed into a
426 sinking airflow when blocked by the high-altitude “warm lid”, which resulted in air
427 pollutant accumulation and completion of the longitudinal vertical circulation.
428 Vertical circulation played an important role in the transport and formation of heavy
429 pollution in the Hunan and Hubei provinces, promoting the north-sourced pollutants
430 to migrate and accumulate towards the Hunan–Hubei Plain. In addition, the stable
431 stratification at mid-high layers inhibited the escape of air pollutants, thereby
432 confining them within the atmospheric boundary layer and promoting rapid
433 accumulation of air pollutants in the plain.



434
 435 Figure 8 The longitudinal cross-sectional distribution of meteorological conditions
 436 synthesised from eight typical pollutant-transport events (112.25 °E–113 °E on
 437 average), where the black flow lines represent longitudinal circulation (synthesised by
 438 v and w , vertical velocity is multiplied by 10), the green contour lines represent wind
 439 speed anomalies (in m s^{-1}), and the colour scale represents temperature anomalies
 440 (in °C).

441
 442 Based on the daily atmospheric sounding data at 00UTC recorded at the Wuhan
 443 station and Changsha station in Hunan and Hubei provinces, vertical sounding
 444 profiles of temperature and wind speed were synthesised from eight typical
 445 pollutant-transport events (Figure 9). It is evident that during pollutant transport, the
 446 surface wind speeds at the Wuhan station reached 5 m s^{-1} ; in near-surface layers
 447 below 950-hPa, wind speeds and air temperature increased and decreased with the
 448 layer height, respectively, indicative of the non-stagnant state of the near-surface
 449 atmospheric structure and the “openness” of the transport channel, which facilitated
 450 the transport of a large amount of pollutants to the Hunan and Hubei provinces. In
 451 contrast, there appeared an obvious temperature inversion layer at 950-900 hPa,
 452 where the wind speeds decreased with height, forming stable atmospheric
 453 stratification which suppressed the vertical diffusion of pollutants during their
 454 transport; at 800-750 hPa, there existed another stable stratified structure, which
 455 confined air pollutant transport within the atmospheric boundary layer. Analysis of the
 456 sounding data from the Changsha station gave a consistent result, but the transport
 457 channel gradually “shrank”. The atmosphere below 975 hPa was in a non-stationary
 458 state. Above 975 hPa, the temperature inversion layer was thin, but the isothermal



layer was thicker.

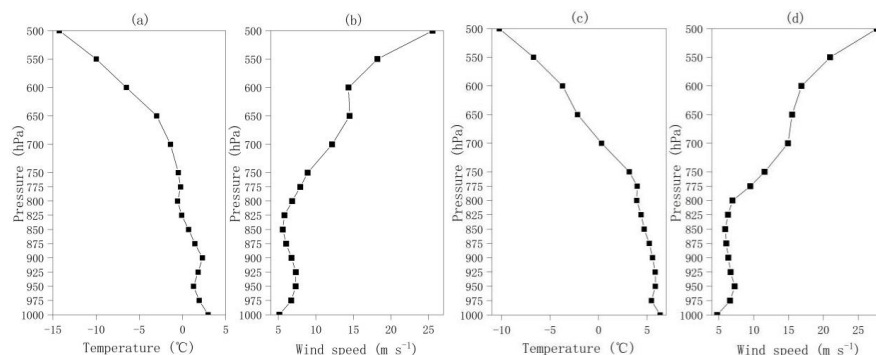


Figure 9 Atmospheric sounding profiles of temperature (a, c) and wind speed (b, d) of the Wuhan station (a, b) and Changsha station (c, d) synthesised from eight typical air pollutant transport events

Regional means of relevant meteorological parameters were calculated separately for the upstream area of Hubei province, Hubei province, and Hunan province and the downstream area of Hunan province to further investigate the vertical variation of meteorological conditions during pollutant transport in different areas (Figure 10). The results showed that in the Hunan and Hubei provinces and their upstream areas, (1) the temperature anomalies below 950 hPa decreased with height, which was consistent with the atmospheric sounding results of the meteorological stations; (2) below 850 hPa, there existed anomalous northerly winds with high speeds, with the atmosphere exhibiting non-stationary characteristics; and (3) at mid-high layers, the temperature anomalies significantly increased with height, where there existed anomalous southerly low-speed winds and stable atmospheric stratification, with anomalous “warm lid” characteristics. The low-altitude wind fields diverged in the Hubei province and its upstream area but converged in the Hunan province and its downstream area, leading to air pollutant transport and accumulation. In the downstream area, the anomalous winds turned south, buffering transport of air pollutants.

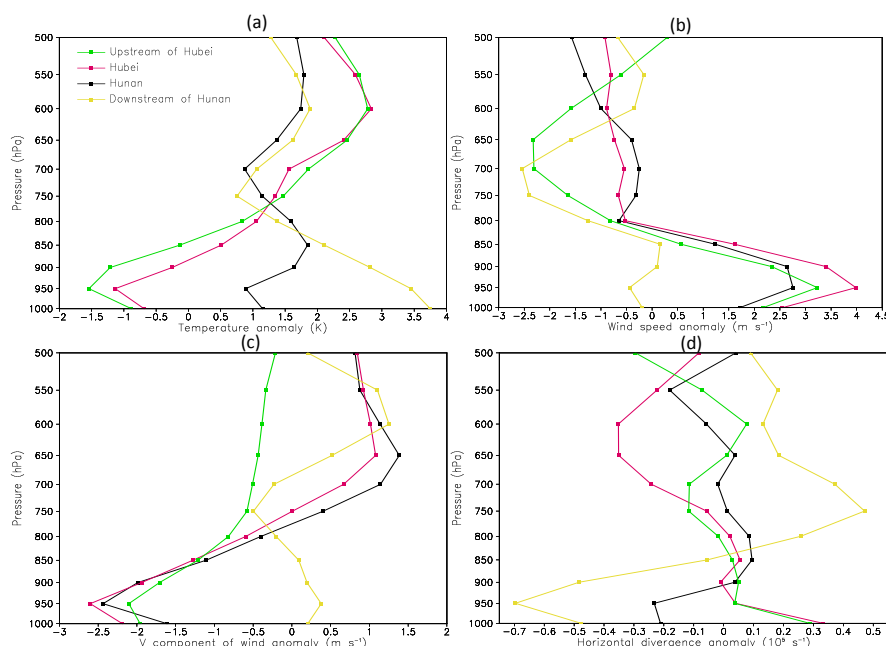


Figure 10 Synthesized vertical profiles of temperature anomaly (a), wind speed anomaly (b), v component of wind anomaly (c), and horizontal divergence anomaly (d) in different geographical areas during eight typical pollutant-transport events, where the green lines represent the upstream area (33–36 °N, 112–118 °E), the red line Hubei province (30–33 °N, 111–116 °E), the black line Hunan province (26–30 °N, 110–114 °E), and the yellow line the downstream area (23–26 °N, 109–115 °E).

As shown above, the mechanisms of meteorological conditions on air pollutant transport and the heavy pollution process in the Hunan and Hubei provinces are the following: (1) the anomalous northerly winds in the near-surface layer of the Hunan and Hubei provinces and their upstream area are accompanied by the southward penetration of a shallow cold layer, which provides dynamic conditions for regional pollution transport; (2) weak cold air degenerates as it passes through the Hunan–Hubei Plain, causing warm air to accumulate in the near-surface layer of the downstream area, where winds slow down and converge, buffering pollutant transport and thereby resulting in pollutant accumulation; (3) the atmosphere in the near-surface layer of the Hunan and Hubei provinces is in a non-stationary state (dry intrusion of cold air, anomalously strong winds, and positive anomalies of boundary-layer height), which is conducive to the horizontal transport of pollutants; (4) the mid-high layers



503 have stable stratification, characterized by temperature inversion and the presence of a
504 “warm lid”, which inhibits the diffusion of pollutants to the upper layers; and (5) there
505 is obvious longitudinal vertical circulation above the Hunan–Hubei Plain, and the
506 regional transport is confined within the atmospheric boundary layer, which results in
507 sinking and accumulation of the pollutants, thereby promoting rapid accumulation of
508 pollutants in the Hunan and Hubei provinces.

509

510 **5 Quasi-4-d periodic oscillation of pollutant transport in the Hunan and Hubei** 511 **provinces**

512 **5.1 Quasi-4-d evolution characteristics of regional transport of PM_{2.5}**

513 Regional transport is associated with the synoptic scale. The East Asian winter
514 monsoon has a short-term 4–6-day cycle of weak cold air activity. Power spectrum
515 analysis revealed that the time coefficient of the regional transport mode had a
516 significant period of 5–6 days, which was associated with the short-term weak cold air
517 activity of the East Asian winter monsoon. To explore the spatial evolution
518 characteristics of the eigenvector of regional pollution transport, EEOF was used to
519 analyse the spatio-temporal field of PM_{2.5} and 10-m wind vector in central China
520 (Hunan and Hubei provinces and the upstream area of the Henan province).

521 To reveal the effect of the short-term cycle of weak cold air activity on regional
522 transport, a second-order Butterworth band-pass filter with a 4–6-day filtering window
523 was applied on a synoptic scale to the time series of PM_{2.5} and 10-m wind vector
524 collected at 48 urban environmental monitoring stations in central China in January
525 2015–2019. Next, the time series of each station with a period of 4–6 days was
526 synthesized to form a data matrix, which was subjected to EEOF decomposition based
527 on a lag time of 2 days. The first two eigenvectors passed the significance test. The
528 first and second eigenvectors of PM_{2.5} (10-m wind vector), referred to as EEOF1 and
529 EEOF2 respectively, cumulatively accounted for 48.9% (37.4%) of the total variance.
530 The eigenvectors described by EEOF1 and EEOF2 represent situations at different
531 instances of time during the periodic process, with EEOF1 leading EEOF2 in phase
532 by a quarter of a period (1 days).

533 The time coefficient of EEOF eigenvectors for PM_{2.5} had a good correlation with
534 that for the 10-m wind vector (Figure 11). The EEOF2 time series of PM_{2.5} was
535 significantly positively correlated with the EEOF1 time series of 10-m wind vector
536 (cor = 0.5), indicative of the driving of regional transport by strong winds; the



537 EEOF1 time series of $PM_{2.5}$ was significantly negatively correlated with the EEOF2
 538 time series of 10-m wind vector (cor = -0.6), indicative of the removal of transported
 539 pollutants by strong winds.

540 Figure 11 illustrates the eigenvectors (i.e., spatial distribution of the eigenvectors
 541 EEOF2 and EEOF1) of $PM_{2.5}$ in the order of increasing time lags, namely 0 day, 1
 542 day, and 2 days for EEOF2, followed by 0 day for EEOF1. The results showed that
 543 the eigenvector of EEOF1 at a 1-day (2-day) (omitted from illustration) time lag was
 544 similar to that of EEOF2 at a 0-day (1-day) time lag, that is, the four eigenvectors
 545 constituted a 4-day oscillation period of the regional transport. Because of the
 546 correlation of EEOF time coefficient between $PM_{2.5}$ and 10-m wind vector, the
 547 eigenvectors of 10-m wind vector were arranged in the order of EEOF1 (sequentially
 548 at time lags of 0, 1, and 2 days) and EEOF2 (at a time lag of 0 d) to correspond to the
 549 above eigenvectors of $PM_{2.5}$.

550 As shown in Figure 11, the EEOF eigenvectors at different time lags reflected the
 551 spatial evolution characteristics of regional air pollutant transport, and the regional
 552 transport had a quasi-4-d oscillation period, with the synoptic situation undergoing the
 553 same evolution as revealed earlier in this study. On the first day, stable meteorological
 554 conditions occurred and weak winds prevailed in the whole region, with air pollutant
 555 accumulation in the upstream area of northern Henan province. On the 2nd day, the
 556 cold air penetrated southward, and the wind speeds in the upstream area increased,
 557 continuously and cumulatively transporting air pollutants to the Hunan and Hubei
 558 provinces, mainly through the Nanxiang Basin and the low hills of the Dabie
 559 Mountain. On the third day, the northerly winds in the Hunan and Hubei provinces
 560 and their upstream area reached maximum speeds, and the near-surface layer was in a
 561 non-stationary state; the air pollutants were transported along two pathways (the
 562 Nanxiang Basin-Yunmeng Plain pathway and the Dabie Mountain's Hilly
 563 Area-Yunmeng Plain pathway) to the Hunan-Hubei Plain, where they accumulated;
 564 Meanwhile, air pollutants in the upstream area of northern Henan province were
 565 removed by strong winds. The mechanism of air pollutant transport and heavy
 566 pollution formation in the Hunan and Hubei provinces has been discussed earlier in
 567 this study. On the fourth day, strong winds continued to influence the upstream area,
 568 where the local pollutants were fully removed, leading to completion of regional
 569 pollutant transport.

570

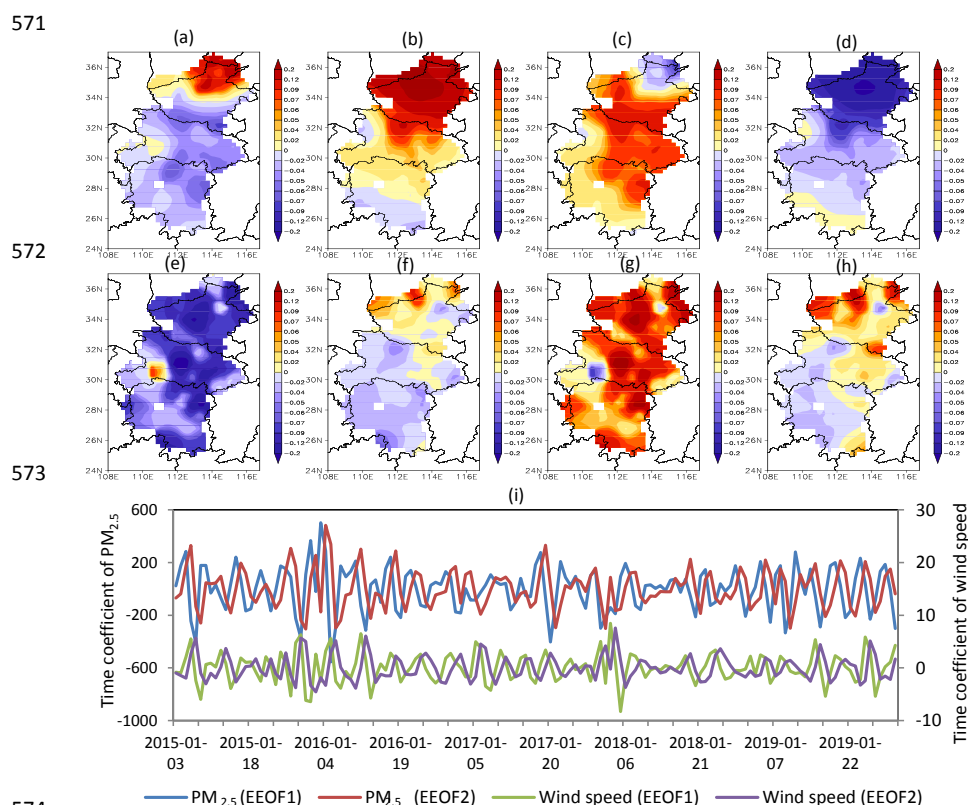


Figure 11 Eigenvectors (a-h) of the EEOF1 and EEOF2 at different time lags for PM_{2.5} and 10-m wind vector during regional pollutant transport and the time coefficients (i). For PM_{2.5}, EEOF2 exhibited time lags of 0 (a), 1 (b), and 2 days (c), and EEOF1 exhibited a time lag of 0 day (d); for the 10-m wind vector, EEOF1 exhibited time lags of 0 d (e), 1 d (f), and 2d (g), and EEOF2 exhibited a time lag of 0 day (h).

5.2 Numerical simulation validation

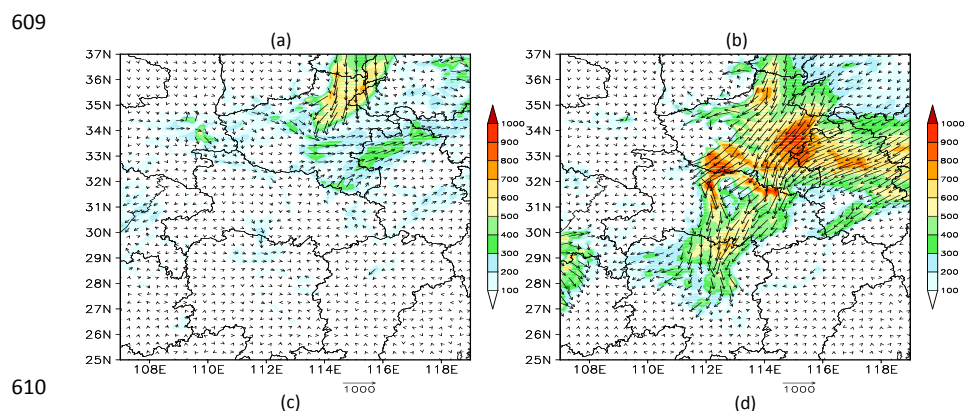
The regional transport event during January 3 and 6, 2016 selected from table 1, which corresponded to the maximum positive values of the EEOF time coefficient, was used WRF-Chem model to simulate pollutant-transport characteristics and meteorological transport conditions in Hunan and Hubei provinces, and a closure experiment was performed on pollutant emission sources to verify the important contribution of regional transport to the rapid accumulation of air pollutants in the Hunan–Hubei Plain.

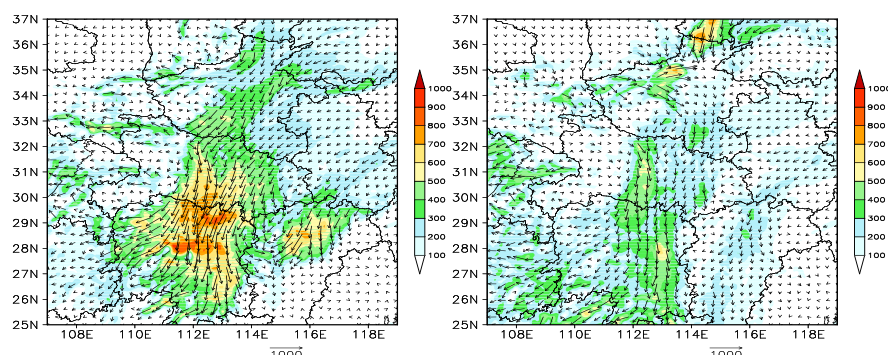
WRF-Chem is a new-generation mesoscale three-dimensional air quality model



(Grell et al., 2005), which is jointly developed by NOAA, NCAR, and UCAR and allows on-line coupling of meteorological conditions and atmospheric chemistry. A central China-specific environmental meteorology numerical model system with the WRF-Chem model as the core component demonstrated good performance in forecast evaluation and application (Bai et al., 2016, 2020), and the scheme for localized testing of the model is documented in detail elsewhere (Bai et al., 2016). The air pollutant transport process during January 3-6, 2016, in the Hunan and Hubei provinces was simulated here by the above numerical model system based on the MIX anthropogenic emissions inventory for Asia in January 2016 (Li et al., 2017b), with the initial and boundary atmospheric conditions set using the NCAR FNL data with a resolution of $1^\circ \times 1^\circ$.

Figure 12 shows the evolving spatial distribution of the regional transport flux of $\text{PM}_{2.5}$ at 00 UTC during January 3-6, 2016. The results indicate that the simulation results were very similar to the EEOF analysis results. The regional pollution transport was subject to a quasi-4-d period consisting of the following sequential events: pollutant accumulation in the upstream calm wind zone, pollutant inputs along the Nanxiang Basin and the hilly area of the Dabie Mountain, pollutant transport and accumulation in the Hunan–Hubei Plain, and dissipation and removal of regional pollution.





611

612 Figure 12 Spatial distribution of the regional transport flux of $\text{PM}_{2.5}$ simulated by the
613 WRF-Chem model (the arrows denote $\text{PM}_{2.5}$ transport flux, and the colour scales
614 denote modulus length in $\mu\text{g m}^{-2} \text{S}^{-1}$) at 00 UTC on January 3 (a), January 4 (b), January
615 5 (c), and January 6 (d) in 2016.

616

617 Figure 13 presents a longitudinal cross-sectional profile of the regional transport
618 pathway within the atmospheric boundary layer along the Hunan–Hubei Plain at
619 different transport times. The results indicated that the main transport pathway of air
620 pollutants was below 1-km height in the atmospheric boundary layer. Air pollutants
621 were inputted and accumulated along the Nanxiang Basin and then transported to the
622 Hunan–Hubei Plain under the driving force of the northerly airflow, whereas the
623 southerly airflow acted as a buffer to prevent air pollutants from moving further
624 southward, which resulted in rapid accumulation of the transported pollutants; the
625 maximum values of $\text{PM}_{2.5}$ transport flux were observed near a height of 400–600 m.
626 The atmosphere below 1-km height in the atmospheric boundary layer of the Huan–
627 Hubei Plain was in a non-stationary state, while there existed obvious isothermal
628 stratification in the atmosphere above the pathway, which limited the upward
629 diffusion of pollutants. The simulation results verified the above-mentioned effect
630 mechanism of meteorological conditions on air pollutant transport and heavy
631 pollution in the Hunan and Hubei provinces.

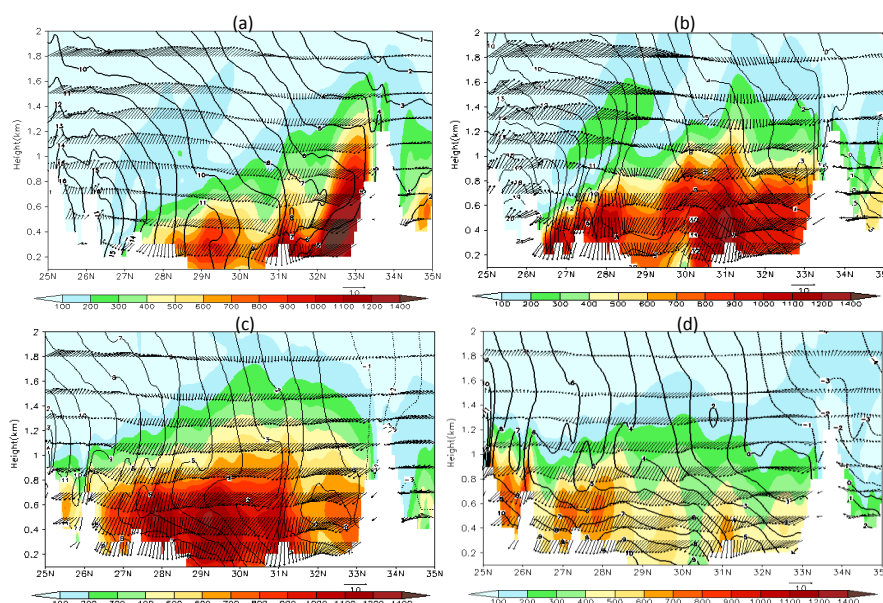


Figure 13 Longitudinal cross-sectional profiles simulated by the WRF-Chem model for pollutant transport along 112.25°E at 00 UTC of January 4 (a), 12 UTC of January 4 (b), 00 UTC of January 5 (c), and 12 UTC of January 5 (d) in 2016, where the colour scales represent $\text{PM}_{2.5}$ transport flux (in $\mu\text{g m}^{-2} \text{s}^{-1}$), the arrows represent horizontal wind fields (in m s^{-1}), and the black contour lines represent temperature (in $^{\circ}\text{C}$).

A closure experiment was conducted by hypothetically shutting down the anthropogenic emission sources in the Hunan and Hubei provinces and simulating the $\text{PM}_{2.5}$ flux component and flux percentage in the two provinces contributed by $\text{PM}_{2.5}$ transport from exogenous sources. Figure 14 presents a simulated time-dependent vertical profile on the Jiangnan Plain in the closure experiment. The results showed that the vertical distribution of pollutants during their transport was affected by the northerly winds in the boundary layer. An increase in wind speed led to an increase in $\text{PM}_{2.5}$ transport, with transport from exogenous sources contributing as high as 60-80% to the near-surface $\text{PM}_{2.5}$ and as high as 80-90% to $\text{PM}_{2.5}$ at a height of 600-900 m, which indicated that the regional transport had a significant promotional effect on pollutant accumulation in the Hunan and Hubei provinces. Because of the instability of near-surface atmospheric layer, the transported exogenous $\text{PM}_{2.5}$ accumulated first on the surface (18-19 UTC on January 4) and then accumulated continuously for 3-4 h



at the bottom of the isothermal layer at a height near 700 m, which indicated that the high-altitude accumulation of transported pollutants was closely related to stable atmospheric stratification.

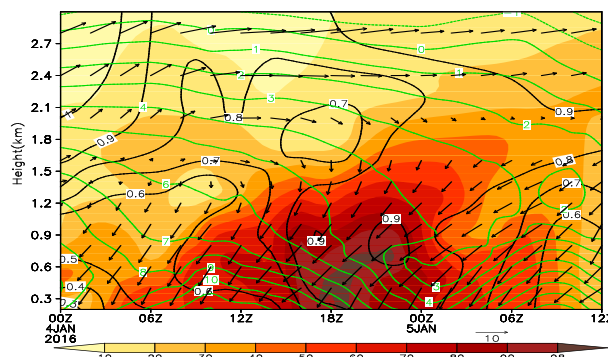


Figure 14 A height-time profile (30°N, 112.25°E) simulated by the WRF-Chem model for pollutant transport after hypothetical closure of the local anthropogenic emission sources of Hunan and Hubei provinces, where the colour scales represent the concentration of PM_{2.5} transported from exogenous sources (in $\mu\text{g m}^{-3}$), the arrows represent horizontal wind fields (in m s^{-1}), the green contour lines represent temperature (in °C), and the black contour lines represent the percent contribution of exogenous sources to PM_{2.5} transport (PM_{2.5} concentration in the closure experiment divided by PM_{2.5} concentration in a control experiment).

6 Conclusions and discussions

The Hunan–Hubei Plain in the middle Yangtze Basin has a special geographical location. It forms a border of China’s areas with the most concentrated atmospheric pollution—the Central Plains, Fenwei Plain, North China Plain, and Yangtze River Delta region—and is located in the downwind direction of the areas of heavy pollution sources under the influence of winter monsoon, serving as a hub for the regional transport of atmospheric pollutants in China. The extent and mechanism of the effect of regional pollutant transport on air pollution in the Hunan–Hubei Plain is a pressing issue in atmospheric environmental science, calling for in-depth investigation. Different from cumulative heavy pollution in central and eastern China, the pollutant transport characteristics and the effect mechanism of meteorological conditions on heavy pollution processes in typical regions like Hunan and Hubei provinces have not been systematically investigated yet.

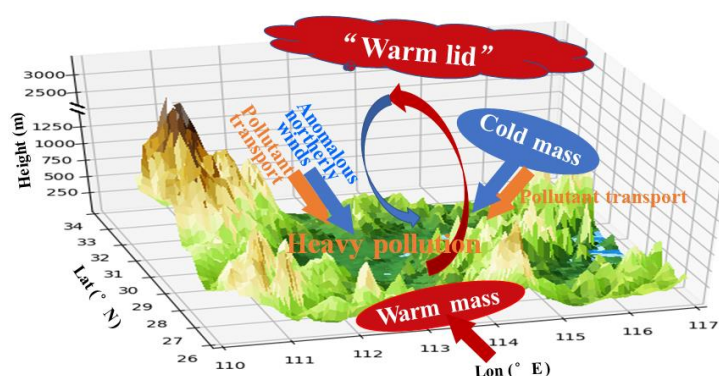


680 Different from the cumulative heavy pollution under unfavourable local
681 meteorological conditions, the atmospherically transported heavy air pollution is
682 under favourable meteorological conditions for horizontal diffusion, that is, the
683 atmospheric boundary layer is high, the wind speeds in the near-surface layer are
684 anomalously high, and the $\text{PM}_{2.5}$ concentration tends to grow rapidly under the
685 influence of strong northerly winds. The MV-EOF method was employed in this study
686 to extract a typical mode of regional pollutant transport, which was characterized by
687 high $\text{PM}_{2.5}$ concentration, south–north pressure gradient, and anomalous northerly
688 winds in the Hunan and Hubei provinces in January 2015–2019. The time coefficient
689 of the MV-EOF mode accounted for 48.4% of the total variance of the average $\text{PM}_{2.5}$
690 concentration in the two provinces, which indicated that regional pollutant transport
691 was almost the dominant factor determining the changes in pollutant concentration in
692 the region; regional transport caused the $\text{PM}_{2.5}$ concentration anomalies in the
693 Wuhan-centred urban agglomeration and the Changsha–Zhuzhou–Xiangtan urban
694 agglomeration to exceed $50 \mu\text{g m}^{-3}$, promoting rapid local accumulation of pollutants
695 in these high-density cities.

696 By synthesizing eight typical pollutant-transport events in Hunan and Hubei
697 provinces in conjunction with surface meteorological observation data, atmospheric
698 sounding data, and reanalysis data, this study comprehensively analyzed the effect
699 mechanism of meteorological conditions on air pollutant transport and accumulation
700 (Figure 15). Transporting air pollutants mainly passed through the Nanxiang Basin
701 and the low hills of the Dabie Mountain. The anomalous northerly winds in the
702 near-surface layer of the Hunan and Hubei provinces and their upstream area were
703 accompanied by southward penetration of a shallow cold layer, which provided
704 dynamic conditions for regional air pollutant transport. The weak cold air degenerates
705 as it passes through the Hunan–Hubei Plain, causing warm air to accumulate in the
706 near-surface layer of the downstream area, where winds slow down and converge,
707 buffering pollutant transport and resulting in pollutant accumulation; the atmosphere
708 in the near-surface layer of the Hunan and Hubei provinces is in a non-stationary state
709 (dry intrusion of cold air, anomalously strong winds, and positive anomalies of
710 boundary-layer height), which is conducive to the horizontal transport of pollutants.
711 The mid-high layers have stable stratification, characterized by temperature inversion
712 and the presence of a "warm lid", which inhibits the diffusion of air pollutants to the
713 upper layers; there is obvious longitudinal vertical circulation above the Hunan–Hubei



714 Plain, which confines the regional transport within the atmospheric boundary layer
 715 where the pollutants sink and accumulate, thereby promoting rapid accumulation of
 716 pollutants in Hunan and Hubei provinces. These results are also verified by numerical
 717 simulations.



718
 719 Figure 15. Meteorological mechanism of regional transport in winter heavy air
 720 pollution events in the middle Yangtze Basin areas over China

721
 722 The activities of weak cold air are crucial for pollutant transport in the Hunan
 723 and Hubei provinces. EEOF analysis revealed that the regional pollutant transport in
 724 the two provinces is subject to a quasi-4-d period consisting of the following
 725 sequential events: pollutant accumulation in the upstream calm wind zone, air
 726 pollutant input along the Nanxiang Basin and the hilly area of the Dabie Mountain,
 727 pollutants transport and accumulation in the Hunan–Hubei Plain, dissipation and
 728 removal of regional pollution; this is associated with the short-term 4-6-day cycle of
 729 weak cold air activity during the East Asian winter monsoon. It is noteworthy that the
 730 continuous accumulation of air pollutants in the upstream area and the sudden
 731 changes of synoptic situation (i.e., a change from a uniform surface pressure field to a
 732 surface high-pressure system whose lower part strongly influences the surface, an
 733 increase of the south–north pressure gradient, and the formation of anomalous
 734 northerly airflow) can be used as a predictive warning sign for air pollutant transport
 735 in the Hunan and Hubei provinces.

736 In addition, from a geographic aspect, the Hunan and Hubei provinces are in a
 737 large exoreic basin, which is bounded by the Jing Mountain, Dahong Mountain, and
 738 Dabie Mountain to the north, the Wuling Mountains to the west, the Mufu Mountain
 739 and Luoxiao Mountain to the east, and the Xuefeng Mountain and its foothills to the



south and has an area of more than 130,000 km². It is necessary to have deeper insights into the concentrating effect of this special sub-basin topography and the underlying surface of the complicated basin on regional air pollutant transport, as well as the mechanism of the multi-scale synergistic effect of local circulation, synoptic situation, and East Asian monsoon climate change on regional air pollutant transport.

Data availability. The data used in this paper can be provided by Yongqing Bai (2007byq@163.com) upon request.

Author contributions. YB, TZ, and YZ conducted the study design. JX, WH, and SK provided the observational data. WH, YG, HZ and LL assisted with data processing. YB wrote the paper with the help of LL and SK. TZ, YZ, JX, LL, and SK were involved in the scientific interpretation and discussion. All authors provided commentary on the paper.

Competing interests. The authors declare that they have no conflict of interest.

Acknowledgment. The authors are grateful to Associate Professor Zhao Shuyun, Department of Atmospheric Sciences, School of Environmental Sciences, China University of Geosciences (Wuhan) for the useful comments on improving the first draft of this paper.

Financial support. This research has been supported by the National Natural Science Foundation of China (grant no. 41830965; 42075186), the National Key Research and Development Project of China (grant no. 2016YFC0203304).

References

- Bai, Y., Qi, H., Liu, L., Cui, C., Lin, C., and Tan, C.: Development and Preliminary Application of Environmental Meteorology Numerical Model System in Central China(in Chinese), Plateau Meteor., 35, 1671-1682, 10.7522/j.issn.1000-0534.2015.00086, 2016.
- Bai, Y., Qi, H., Zhao, T., Zhou, Y., Liu, L., Xiong, J., Zhou, Z., Cui, C.: Simulation of the responses of rainstorm in the Yangtze River Middle Reaches to changes in anthropogenic aerosols emissions. Atmos. Environ., 220, 117081, 10.1016/j.atmosenv.2019.117081, 2020.
- Chen, L., Zhu, J., Liao, H., Gao, Y., Qiu, Y., Zhang, M., Liu, Z., Li, N., and Wang, Y.: Assessing the



776 formation and evolution mechanisms of severe haze pollution in the Beijing–Tianjin–Hebei region
 777 using process analysis, *Atmos. Chem. Phys.*, 19, 10845–10864, 10.5194/acp-19-10845-2019, 2019.
 778 Cheng, J., Su, J., Cui, T., Li, X., Dong, X., Sun, F., Yang, Y., Tong, D., Zheng, Y., Li, Y., Li, J., Zhang, Q., and
 779 He, K.: Dominant role of emission reduction in PM 2.5 air quality improvement in Beijing during 2013–
 780 2017: a model-based decomposition analysis. *Atmos. Chem. Phys.* 19, 6125–
 781 6146.10.5194/acp-19-6125-2019, 2019.
 782 Ding, A., Huang, X., Nie, W., Chi, X., Xu, Z., Zheng, L., Xu, Z., Xie, Y., Qi, X., Shen, Y., Sun, P., Wang, J., Gao,
 783 M., Carmichael, G. R., Wang, Y., Saide, P. E., Yu, M., Xin, J., Liu, Z., and Wang, Z.: Modeling study of the
 784 2010 regional haze event in the North China Plain, *Atmos. Chem. Phys.*, 16, 1673–1691,
 785 10.5194/acp-16-1673-2016, 2016.
 786 Ding, Y., Wu, p., Liu, Y., Song, Y.: Environmental and Dynamic Conditions for the Occurrence of
 787 Persistent Haze Events in North China, *Engineering*, 3, 266–271, 10.1016/J.ENG.2017.01.009, 2017.
 788 Grell, G. A., Peckham, S. E., Schmitz, R., McKeen, S. A., Frost, G., Skamarock, W. C., and Eder, B.: Fully
 789 coupled “online” chemistry within the WRF model, *Atmos. Environ.*, 39, 6957–6975,
 790 10.1016/j.atmosenv.2005.04.027, 2005.
 791 Guo, J., He, J., Liu, H., Miao, Y., Liu, H., and Zhai, P.: Impact of various emission control schemes on air
 792 quality using WRF-Chem during APEC China 2014, *Atmos. Environ.*, 140, 311–319,
 793 10.1016/j.atmosenv.2016.05.046, 2016a.
 794 Guo, J., Miao, Y., Zhang, Y., Liu, H., Li, Z., Zhang, W., He, J., Lou, M., Yan, Y., Bian, L., and Zhai, P.: The
 795 climatology of planetary boundary layer height in China derived from radiosonde and reanalysis data,
 796 *Atmos. Chem. Phys.*, 16, 13309–13319, 10.5194/acp-16-13309-2016, 2016b.
 797 Guo, J., Li, Y., Cohen, J. B., Li, J., Chen, D., Xu, H., Liu, L., Yin, J., Hu, K., and Zhai, P.: Shift in the temporal
 798 trend of boundary layer height in China using long - term (1979 – 2016) radiosonde data. *Geophys.*
 799 *Res. Lett.*, 46, 6080–6089. <https://doi.org/10.1029/2019GL082666>, 2019.
 800 Huang, X. Ding, A., Wang, Z., Ding, K. Gao, J., Chai, F., and Fu, C.: Amplified transboundary transport
 801 of haze by aerosol-boundary layer interaction in China, *Nat. Geosci.*, 13, 428–434,
 802 doi:10.1038/s41561-020-0583-4, 2020.
 803 Kan, H., Chen, R., and Tong, S.: Ambient air pollution, climate change, and population health in China,
 804 *Environ. Int.*, 42, 10–19, 10.1016/j.envint.2011.03.003, 2012.
 805 Kang, H., Zhu, B., Gao, J., He, Y., Wang, H., Su, J., Pan, C., Zhu, T., and Yu, B.: Potential impacts of cold
 806 frontal passage on air quality over the Yangtze River Delta, China, *Atmos. Chem. Phys.*, 19, 3673–3685,
 807 10.5194/acp-19-3673-2019, 2019.
 808 Khuzestani, R.B., Schauer, J. J., Wei, Y., Zhang, L., Cai, T., Zhang, Y., Zhang, Y.: Quantification of the
 809 sources of long-range transport of PM2.5 pollution in the Ordos region, Inner Mongolia, China,
 810 *Environ. Pollut.*, 229, 1019–1031, 10.1016/j.envpol.2017.07.093, 2017.
 811 Kim, C.-H., Park, S.-Y., Kim, Y.-J., Chang, L.-S., Song, S.-K., Moon, Y.-S., and Song, C.-K.: A numerical
 812 study on indicators of long-range transport potential for anthropogenic particulate matters over
 813 northeast Asia, *Atmos. Environ.*, 58, 35–44, 10.1016/j.atmosenv.2011.11.002, 2012.
 814 Li, J., Du, H., Wang, Z., Sun, Y., Yang, W., Li, J., Tang, X., and Fu, P.: Rapid formation of a severe regional
 815 winter haze episode over a mega-city cluster on the North China Plain, *Environ. Pollut.*, 223, 605–615,
 816 10.1016/j.envpol.2017.01.063, 2017a.
 817 Li, M., Zhang, Q., Kurokawa, J.-i., Woo, J.-H., He, K., Lu, Z., Ohara, T., Song, Y., Streets, D. G., Carmichael,
 818 G. R., Cheng, Y., Hong, C., Huo, H., Jiang, X., Kang, S., Liu, F., Su, H., and Zheng, B.: MIX: a mosaic Asian
 819 anthropogenic emission inventory under the international collaboration framework of the MICS-Asia



820 and HTAP, *Atmos. Chem. Phys.*, 17, 935–963, 10.5194/acp-17-935-2017, 2017b.
 821 Li, M., Yuan, K., Hu, K., and Liu, W.: Trigger mechanism and main factors of urban heavy pollution
 822 processes in Wuhan(in Chinese). *Torrential Rain Disaster.*, 38(6), 624–631.
 823 10.3969/j.issn.1004-9045.2019.06.007, 2019.
 824 Li, R., Mei, X., Wei L., Han, X., Zhang, M., Jing, Y.: Study on the contribution of transport to PM_{2.5} in
 825 typical regions of China using the regional air quality model RAMS-CMAQ, *Atmos. Environ.*, 214,
 826 116856, <https://doi.org/10.1016/j.atmosenv.2019.116856>, 2019.
 827 Lu, M., Tang, X., Wang, Z., Gbaguidi, A., Liang, S., Hu, K., Wu, L., Wu, H., Huang, Z., and Shen, L.:
 828 Source tagging modeling study of heavy haze episodes under complex regional transport processes
 829 over Wuhan megacity, Central China. *Environ. Pollut.*, 231, 612–621, 10.1016/j.envpol.2017.08.046,
 830 2017.
 831 Lu, Y., Wang, Y., Zhang, W., Klaus, H., Bi, F., Zuo, J., Jiang, H., Zhang Z., Feng, K., Liu, Y., and Xue., W.:
 832 Provincial air pollution responsibility and environmental tax of China based on interregional linkage
 833 indicators, *J. Clean. Prod.*, 235, 337–347, 10.1016/j.jclepro.2019.06.293, 2019a.
 834 Lu, M., Tang, X., Wang, Z., Wu, L., Chen, X., Liang, S., Zhou, H., Wu, H., Hu, K., Shen, L., Yu, J., and Zhu,
 835 J.: Investigating the Transport Mechanism of PM_{2.5} Pollution during January 2014 in Wuhan, Central
 836 China, *Adv. Atmos. Sci.*, 36, 1217–1234, 10.1007/s00376-019-8260-5, 2019b.
 837 Miao, Y., Guo, J., Liu, S., Liu, H., Li, Z., Zhang, W., and Zhai, P.: Classification of summertime synoptic
 838 patterns in Beijing and their associations with boundary layer structure affecting aerosol pollution,
 839 *Atmos. Chem. Phys.*, 17, 3097–3110, 10.5194/acp-17-3097-2017, 2017.
 840 Ning, G., Wang, S., Yim, S. H. L., Li, J., Hu, Y., Shang, Z., Wang, J., and Wang, J.: Impact of low-pressure
 841 systems on winter heavy air pollution in the northwest Sichuan Basin, China, *Atmos. Chem. Phys.*, 18,
 842 13601–13615, 10.5194/acp-18-13601-2018, 2018.
 843 Tai, A. P. K., Mickley, L. J., and Jacob, D. J.: Impact of 2000–2050 climate change on fine particulate
 844 matter (PM_{2.5}) air quality inferred from a multi-model analysis of meteorological modes. *Atmos. Chem.*
 845 *Phys.*, 12, 11329–11337, 10.5194/acp-12-11329-2012, 2012.
 846 Wang, Y., Yao, L., Wang, L., Liu, Z., Ji, D., Tang, G., Zhang, J., Sun, Y., Hu, B., and Xin, J.: Mechanism for
 847 the formation of the January 2013 heavy haze pollution episode over central and eastern China, *Sci.*
 848 *China Earth Sci.*, 57, 14–25, 10.1007/s11430-013-4773-4, 2013a.
 849 Wang, Z., Li, J., Wang, Z., Yang, W., Tang, X., Ge, B., Yan, P., Zhu, L., Chen, X., Chen, H., Wand, W., Li, J.,
 850 Liu, B., Wang, X., Wand, W., Zhao, Y., Lu, N., and Su, D.: Modeling study of regional severe hazes over
 851 mid-eastern China in January 2013 and its implications on pollution prevention and control, *Sci. China*
 852 *Earth Sci.*, 57, 3–13, 10.1007/s11430-013-4793-0, 2013b.
 853 Wu, D., Fung, J. C. H., Yao, T., and Lau, A. K. H.: A study of control policy in the Pearl River Delta region
 854 by using the particulate matter source apportionment method, *Atmos. Environ.*, 76, 147–161,
 855 10.1016/j.atmosenv.2012.11.069, 2013a.
 856 Wu, J., Guo, J., and Zhao, D.: Characteristics of aerosol transport and distribution in East Asia, *Atmos.*
 857 *Res.*, 132–133, 185–198, 10.1016/j.atmosres.2013.05.018, 2013b.
 858 Xiao, Z., Miao, Y., Du, X., Tang, W., Yu, Y., Zhang, X., Che, H.: Impacts of regional transport and
 859 boundary layer structure on the PM_{2.5} pollution in Wuhan, Central China, *China. Atmos. Environ.*, 230,
 860 117508, 10.1016/j.atmosenv.2020.117508, 2020.
 861 Xu, J., Chang, L., Qu, Y., Yan, F., Wang, F., Fu, Q.: The meteorological modulation on PM_{2.5} interannual
 862 oscillation during 2013 to 2015 in Shanghai, China. *Sci. Total Environ.*, 572, 1138–1149,
 863 10.1016/j.scitotenv.2016.08.024, 2016.



864 Xu, X., Zhao, T., Liu, F., Gong, S. L., Kristovich, D., Lu, C., Guo, Y., Cheng, X., Wang, Y., and Ding, G.:
 865 Climate modulation of the Tibetan Plateau on haze in China, *Atmos. Chem. Phys.*, 16, 1365-1375,
 866 10.5194/acp-16-1365-2016, 2016.

867 Yang, Y., Yim, S. H. L., Haywood, J., Osborne, M., Chan, J. C. S., Zeng, Z., Cheng, J. C. H.: Characteristics
 868 of heavy particulate matter pollution events over Hong Kong and their relationships with vertical wind
 869 profiles using high - time - resolution Doppler lidar measurements. *J. Geophys. Res.-Atmos.*, 124,
 870 9609–9623, 10.1029/2019JD031140, 2019.

871 Yuan, C., Lau, W. K. M., Li, Z., and Cribb, M.: Relationship between Asian monsoon strength and
 872 transport of surface aerosols to the Asian Tropopause Aerosol Layer (ATAL): interannual variability and
 873 decadal changes, *Atmos. Chem. Phys.*, 19, 1901-1913, 10.5194/acp-19-1901-2019, 2019.

874 Yue, Y., Wang, X., Zhang, M., Cao, W., Zhou, Y., Chen, S., and Zhu, Y.: Air quality condition in Wuhan and
 875 its relationship to meteorological factors(in Chinese). *Torrential Rain Disaster.*, 35(3), 271–278.
 876 10.3969/j.issn.1004-9045.2016.03.010,2016.

877 Yu, C., Zhao, T., Bai, Y., Zhang, L., Kong, S., Yu, X., He, J., Cui, C., Yang, J., You, Y., Ma, G., Wu, M., and
 878 Chang, J. : Heavy air pollution with a unique “non-stagnant” atmospheric boundary layer in the
 879 Yangtze River middle basin aggravated by regional transport of PM_{2.5} over
 880 China. *Atmos. Chem. Phys.*, 20, 7217–7230. 10.5194/acp-20-7217-2020,2020.

881 Zhang, J., Zhu, T., Zhang, Q., Li, C., Shu, H., Ying, Y., Dai, Z., Wang, X., Liu, X., Liang, A., Shen, H., and Yi,
 882 B.: The impact of circulation patterns on regional transport pathways and air quality over Beijing and
 883 its surroundings, *Atmos. Chem. Phys.*, 12, 5031-5053, 10.5194/acp-12-5031-2012, 2012a.

884 Zhang, X., Wang, Y., Niu, T., Zhang, X., Gong, S., Zhang, Y., and Sun, J.: Atmospheric aerosol
 885 compositions in China: spatial/temporal variability, chemical signature, regional haze distribution and
 886 comparisons with global aerosols, *Atmos. Chem. Phys.*, 12, 779-799, 10.5194/acp-12-779-2012,
 887 2012b.

888 Zhang, X., Wang, J., Wang, Y., Liu, H., Sun, J., and Zhang, Y.: Changes in chemical components of
 889 aerosol particles in different haze regions in China from 2006 to 2013 and contribution of
 890 meteorological factors, *Atmos. Chem. Phys.*, 15, 12935-12952, 10.5194/acp-15-12935-2015, 2015.

891 Zhang, X., Zhong, J., Wang, J., Wang, Y., and Liu, Y.: The interdecadal worsening of weather conditions
 892 affecting aerosol pollution in the Beijing area in relation to climate warming, *Atmos. Chem. Phys.*, 18,
 893 5991-5999, 10.5194/acp-18-5991-2018, 2018.

894 Zhang, X., Xu, X., Ding, Y., Liu, Y., Zhang, H., Wang, Y., and Zhong, J.: The impact of meteorological
 895 changes from 2013 to 2017 on PM_{2.5} mass reduction in key regions in China, *Sci. China Earth Sci.*,
 896 10.1007/s11430-019-9343-3, 2019.

897 Zhao, X., Zhao, P., Xu, J., Meng, W., Pu, W., Dong, F., He, D., and Shi, Q.: Analysis of a winter regional
 898 haze event and its formation mechanism in the North China Plain, *Atmos. Chem. Phys.*, 13, 5685-5696,
 899 10.5194/acp-13-5685-2013, 2013.

900
 901
 902